Multiple scattering events of primary electrons in directional elastic peak electron spectroscopy

I. Morawski and M. Nowicki*
Institute of Experimental Physics, University of Wrocław, pl. Maxa Borna 9, 50-204 Wrocław, Poland
(Received 24 November 2006; published 12 April 2007)

The application of multiple scattering (MS) calculations is presented in order to describe the scattering process of the primary electron beam in crystalline samples and obtain theoretical directional elastic peak electron spectroscopy (DEPES) profiles. Succeeding scattering orders were considered in MS calculations. The contribution of particular sample layers to the calculated intensities is discussed considering forward focusing, attenuation, and defocusing of primary electrons in the crystalline sample. The calculations were performed for a single [110] chain of Al, Cu, Ag, and Au atoms. The results show the importance of multiple scattering events in DEPES profiles. A reduction of the calculated intensities for the [110] direction was observed when the multiple scattering of primaries was considered. Convergence of the recursion method of MS evaluations for the increasing scattering order was ensured by means of $1/\sqrt{N}$ normalization factor, where N is the number of cluster atoms taken into account. Above the fourth scattering order, no significant changes of the calculated intensities were observed for all the considered kinds of atoms. Theoretical DEPES profiles obtained for the Au(111) crystal show a similar reduction of intensities for the [110] atomic row as was observed for a single Au[110] chain. The consideration of MS events in calculations improve the correspondence between experimental and theoretical DEPES scans for Cu(111) at E_P=1.2 keV.

DOI: 10.1103/PhysRevB.75.155412 PACS number(s): 91.60.Ed, 91.55.Nc

I. INTRODUCTION

Primary electrons striking a crystalline sample undergo strong scattering processes. To describe the scattering of electrons, different theoretical approaches were considered in the literature. The so-called two-beam approximation[1] was used to interpret the scanning electron microscope patterns[2,3] associated with channeling[4] and/or the Kikuchi effect.[5] The incident beam diffraction effects were described also by the many-wave dynamic approximation.[6] Enhancements of the measured signal observed when the collimated beam passed through the closely packed rows of atoms, associated with the forward focusing[7] of primary electrons, were described by the single scattering cluster (SSC) approximation.[8,9]

A more realistic approach than the SSC concerns multiple scattering events which become dominant for large electron energies. The importance of multiple scattering has been reported for high-energy photoelectrons and Auger electrons[10,11] emitted from crystalline samples and observed with the use of x-ray photoelectron diffraction (XPD) and Auger electron diffraction (AED). The defocusing of emitted electrons leads to the suppression of forward scattering intensities. Multiple scattering (MS) calculations performed for a linear chain of atoms show that already a few atoms in the line can suppress the calculated intensities.[12] The experimental evidence of such defocusing was reported by Egelhoff.[13]

In the case of directional elastic peak electron spectroscopy (DEPES),[14] the energy dependent inelastic mean free path of the primary beam governs the penetration depth of primaries in the sample, which can reach several atomic layers. In view of this fact the multiple scattering of primary electrons is expected not to be negligible for energies of several hundreds eV. Theoretical DEPES profiles obtained with the use of SSC calculations reveal intensive [110] maxima.[9,15,16] Multiple scattering leads to the defocusing of the primary beam along the close-packed rows of atoms. Therefore, a reduction of the calculated intensities corresponding to the close-packed directions in DEPES profiles is expected, which can lead to better correspondence between theoretical and experimental results.

In the literature, the MS approach for spherical electron waves was reported in the context of XPD and AED.[12,17–21] The goal of this work is to introduce the multiple scattering formalism for an incident plane wave associated with primary electrons striking a crystalline sample and obtain theoretical DEPES profiles. Succeeding scattering orders of the primary wave were taken into account. The MS calculations were performed for a single [110] atomic chain composed of Al, Cu, Ag, and Au atoms, as well as for a Au(111) crystal. A comparison of experimental and theoretical results is presented for Cu(111).

II. EXPERIMENT

Since the experimental details were presented in many publications,[9,14–16] only a short outline is given in this paper. The measurements were performed with the use of a retarding field analyzer (RFA). In DEPES the primary electron beam was directed onto the crystalline sample and the intensity of elastically backscattered electrons was measured in the normal mode as a function of the incidence angle of the primaries. The incidence angle was changed by the rotation of the sample around the axis parallel to the sample surface. The required azimuth was chosen by rotating the sample around the axis perpendicular to the surface. The experimental scan was recorded along the $[11\bar{2}]$ azimuth of the Cu(111) sample for the primary electron beam energy E_P =1.2 keV.

III. MS THEORY

The multiple scattering of the primary beam was introduced for a more realistic description of the diffraction ef-

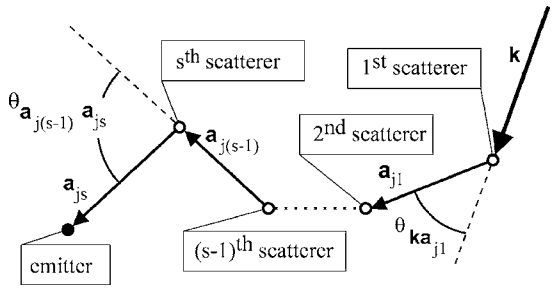

FIG. 1. Scattering model used in MS calculations for an incident plane wave with wave vector $\boldsymbol{k}$. The vectors $\boldsymbol{a}_{j1},\ldots,\boldsymbol{a}_{j(s-1)}$ define the relative position of scattering atoms, the vector $\boldsymbol{a}_{js}$ indicates the position of the emitter with respect to the sth scatterer, and s is the highest scattering order taken into account.

fects of primary electrons in the crystalline sample. Similarly to the SSC approach, the small atom approximation[22] was used and the incident wave was considered to be a plane wave with the propagation vector $\boldsymbol{k}$. The wave function of the elastically scattered electrons at the emitter site $\boldsymbol{r}_n$ in the crystal written in MS approximation is given by

$$\Psi(\boldsymbol{k},\boldsymbol{r}_n,s)=\psi^0(\boldsymbol{k},\boldsymbol{r}_n)+\psi^1(\boldsymbol{k},\boldsymbol{r}_n)+\psi^2(\boldsymbol{k},\boldsymbol{r}_n)+\cdots+\psi^s(\boldsymbol{k},\boldsymbol{r}_n), \tag{1}$$

where the upper index describes the MS order and s denotes the highest scattering order taken into account. In this equation $\psi^0(\boldsymbol{k},\boldsymbol{r}_n)$ is the wave function of primary electrons; $\psi^1(\boldsymbol{k},\boldsymbol{r}_n),\ldots,\psi^s(\boldsymbol{k},\boldsymbol{r}_n)$ represent the wave functions associated with the single scattering and higher scattering orders, respectively. The explicit form of the s-fold scattered wave function at the emitter site $\boldsymbol{r}_n$ can be written in the MS approach as

$$\Psi^s(\boldsymbol{k},\boldsymbol{r}_n)=\left(\frac{1}{\sqrt{N}}\right)^s e^{i\boldsymbol{k}\boldsymbol{r}_n}\times\sum_{\boldsymbol{a}_{j1}}\sum_{\boldsymbol{a}_{j2}}\cdots\sum_{\boldsymbol{a}_{js}}e^{-i\boldsymbol{k}(\boldsymbol{a}_{j1}+\boldsymbol{a}_{j2}+\cdots+\boldsymbol{a}_{js})}\times\left(\frac{e^{ika_{j1}}}{a_{j1}}\frac{e^{ika_{j2}}}{a_{j2}}\cdots\frac{e^{ika_{js}}}{a_{js}}\right)(f_{\boldsymbol{k}\boldsymbol{a}_{j1}}f_{\boldsymbol{a}_{j1}\boldsymbol{a}_{j2}}\cdots f_{\boldsymbol{a}_{j(s-1)}\boldsymbol{a}_s}). \tag{2}$$

The wave vector $\boldsymbol{k}$ and bond vectors $\boldsymbol{a}_{j1},\ldots,\boldsymbol{a}_{js}$ used in Eq. (2) are shown in Fig. 1. The term $e^{i\boldsymbol{k}\boldsymbol{r}_n}$ multiplied by $e^{-i\boldsymbol{k}(\boldsymbol{a}_{j1}+\boldsymbol{a}_{j2}+\cdots+\boldsymbol{a}_{js})}$ represents the incident plane wave at the beginning of the chain of bond vectors $\boldsymbol{a}_{j1},\ldots,\boldsymbol{a}_{js}$, and e^{ika_j}/a_j is the spherical wave with origin at the beginning of the bond vector $\boldsymbol{a}_j$. The term $1/\sqrt{N}$ is the normalization factor for the number of cluster atoms N. Let us consider one atom (first scatterer) and a certain site $\boldsymbol{r}$ where the total wave function was calculated. At this site $\boldsymbol{r}$ the wave function can be expressed as the sum of the unscattered incident plane wave and the wave scattered by the first scatterer.[23] However, the latter does not represent any additional charge in our system because the solution of the Schrödinger equation includes both unscattered and scattered parts. Now, let us extend our system by adding the second scatterer and considering the scattering of the previously scattered wave. According to the well-known treatment of scattering on two centers of potential as two separate succeeding events, we can solve the Schrödinger equation for the second scattering with the incident wave as the scattered wave originating from the first scatterer. However, such an approach "generates" an additional charge in this system. When we consider all second-order scatterers, the additional charge becomes equal to the number of these scatterers. Considering the next-order scattering up to s we conclude that the additional charge is proportional to the number of scatterers to power s. Hence, we introduce the factor $(1/\sqrt{N})^s$ in Eq. (2), where the exponent arises from the s-fold sum.

In Eq. (2) the sums extend over all scattering atoms in the cluster. Only these scattering events are taken into account for which successive scatterers are different. It that assures $\boldsymbol{a}_j\neq\boldsymbol{0}$. The terms[24] $f_{\boldsymbol{k}\boldsymbol{a}_{j1}}$ and $f_{\boldsymbol{k}\boldsymbol{a}_{j(s-1)}\boldsymbol{a}_{js}}$ are the scattering factors associated with the first and higher scattering orders, respectively. These factors involve the scattering amplitude, the temperature-dependent phase shifts calculated in a muffin-tin approximation,[23,25,26] and the curved wave fronts at the site $\boldsymbol{a}_{j1}$.[27] For the first scattering event of the incident plane wave, the scattering factor can be expressed as follows:[17]

$$f_{\boldsymbol{k}\boldsymbol{a}_{j1}}=\frac{1}{ik}\sum_l(2l+1)T_{l,\boldsymbol{a}_{j1}}(k)d_l(ka_{j1})P_l(\cos\theta_{\boldsymbol{k}\boldsymbol{a}_{j1}}). \tag{3}$$

For further scattering events, the scattering factor can be written as

$$f_{\boldsymbol{a}_{j(s-1)}\boldsymbol{a}_{js}}=\frac{1}{ik}\sum_l(2l+1)T_{l,\boldsymbol{a}_{js}}(k)d_l(ka_{js})\times d_l(ka_{j(s-1)})P_l(\cos\theta_{\boldsymbol{a}_{j(s-1)}\boldsymbol{a}_{js}}), \tag{4}$$

which includes approximations of spherical harmonics of both incoming and outcoming waves.[24]

In Eqs. (3) and (4), $T_{l,\boldsymbol{a}_{js}}(k)=i\sin\delta_l e^{i\delta_l}$ describes the scattering amplitude and the vibrational properties of the scattering atoms by means of the partial-wave phase shifts δ_l[23] for an atom assigned by the bond vector $\boldsymbol{a}_{js}$, $P_l(\cos\theta_{\boldsymbol{k}\boldsymbol{a}_{j1}})$ and $P_l(\cos\theta_{\boldsymbol{a}_{j(s-1)}\boldsymbol{a}_{js}})$ are the lth Legendre polynomials of the cosine of the scattering angles for the first and higher scattering orders, respectively, and $d_j(ka_j)$ is the polynomial part of the Henkel function written as a recursion formula[17]

$$d_l(ka_j)=d_{l-2}(ka_j)-\frac{2l+1}{ika_j}d_{l-1}(ka_j),$$

$$d_0=1,\quad d_1=1+\frac{i}{ka_j}. \tag{5}$$

$|f|^2$ is the elastic scattering cross section for $ka_j\to\infty$, which is the largest at small scattering angles. With the choice of the parameter s in Eqs. (1) and (2) the maximum scattering order is defined.

The MS iterative procedure of computation was performed with the use of the recursion method; therefore, the final wave function at the emitter site $\boldsymbol{r}_n$ can be expressed as follows:

$$\Psi(\boldsymbol{k},\boldsymbol{r}_n,s) = e^{i\boldsymbol{k}\boldsymbol{r}_n}\Bigg\{1 + \sum_{\boldsymbol{a}_{js}} e^{-i\boldsymbol{k}\boldsymbol{a}_{js}}\frac{e^{ika_{js}}}{a_{js}} \times \Bigg[f_{\boldsymbol{k}\boldsymbol{a}_{js}} + \frac{1}{\sqrt{N}}\sum_{\boldsymbol{a}_{j(s-1)}} e^{-i\boldsymbol{k}\boldsymbol{a}_{j(s-1)}}\frac{e^{ika_{j(s-1)}}}{a_{j(s-1)}} f_{\boldsymbol{a}_{j(s-1)}\boldsymbol{a}_{js}} \times \Bigg(f_{\boldsymbol{k}\boldsymbol{a}_{j(s-1)}} + \frac{1}{\sqrt{N}}\sum_{\boldsymbol{a}_{j(s-2)}} e^{-i\boldsymbol{k}\boldsymbol{a}_{j(s-2)}}\frac{e^{ika_{j(s-2)}}}{a_{j(s-2)}} \times f_{\boldsymbol{a}_{j(s-2)}\boldsymbol{a}_{j(s-1)}}(f_{\boldsymbol{k}\boldsymbol{a}_{j(s-2)}} + \cdots)\Bigg)\Bigg]\Bigg\}, \quad (6)$$

where the plus sign in each bracket commences the contribution of the next scattering order. The calculated intensity of elastically backscattered electrons integrated over the large acceptance angle of the analyzer is proportional to the sum of the primary beam intensities over all emitters in the crystalline sample weighted with the escape probability of the outcoming electrons B:[8,28]

$$I(\boldsymbol{k},s) = \sum_{n=1}^{N} |\Psi(\boldsymbol{k},\boldsymbol{r}_n,s)|^2 B\left(\frac{\xi_{r_n}}{\lambda_{out}},\theta_k\right). \quad (7)$$

In calculations, a real experimental geometry was considered, concerning the acceptance angle of the collector and the sample polar rotation with respect to the fixed RFA analyzer.[14,15] The escape probability of the outcoming electrons, B, which takes into account their damping along the way toward the surface, is governed by the emitter distance from the surface ξ_{r_n}, the inelastic mean free path of the outcoming electrons λ_{out}, and the incidence angle θ_k of the primary electron beam:

$$B\left(\frac{\xi_{r_n}}{\lambda_{out}},\theta_k\right) = 2\pi\int_{-\theta_{RFA}}^{\theta_{RFA}} d\theta \exp\left(\frac{\xi_{r_n}}{\lambda_{out}}\frac{1}{\cos(\theta_k+\theta)}\right), \quad (8)$$

where $2\theta_{RFA}$ is the acceptance angle of the retarding field analyzer, here equal to 110°. The probability B was numerically calculated for the ratio ξ_{r_n}/λ_{out} in the range of 0–5. In view of the fact that in experiments the electron gun axis overlaps the RFA axis, the incidence angles θ_k considered were in the range of 0°–80° with respect to the surface normal.

TABLE I. Set of geometric and physical parameters taken in MS calculations. The last row presents mean defocusing values calculated with the use of the formula $100\% \times (I_{SS}-I_{MS})/I_{SS}$ (see text).

	Element			
Property	Al	Cu	Ag	Au
Atomic number	13	29	47	79
Atomic mass	27	64	108	197
Lattice constant (Å)	4.05	3.62	4.09	4.08
Bond distance (Å)	2.86	2.56	2.89	2.88
IMFP at 1 keV (Å)	19.6	16.3	14.2	13.0
No. of atoms in chain	49	44	35	31
Mean defocusing (%)	3	14	32	41

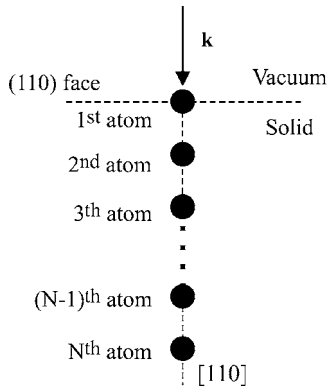

FIG. 2. [110] chain of atoms considered in MS calculations.

The inelastic scattering of the incident electrons within the solid was taken into account by multiplying both the incident plane and the spherical wave functions in Eq. (2) by $e^{-\xi/\lambda}$. The attenuation length ξ of the electrons is a sum of the distance from the surface along the direction of the incident beam to the first scatterer and the distances between successive scatterers, where λ is the inelastic mean free path.

The MS calculations were based on Eqs. (1)–(8) by taking appropriate phase shifts of given atoms, including vibrations at 300 K, and the values of the inelastic mean free paths (IMFPs) at 1 keV. For example, λ for Cu was chosen to be 16.3 Å.[29] Other parameters used in the calculations are shown in Table I.

IV. RESULTS AND DISCUSSION

In MS calculations we considered single [110] chains of Al, Cu, Ag, and Au atoms (Fig. 2) and calculated the contribution of particular emitters to the total intensity of elastically backscattered electrons for the zeroth, first, second, up to ninth maximum scattering order [parameter s in Eq. (6)]. The calculations were performed for the fixed incident direc-

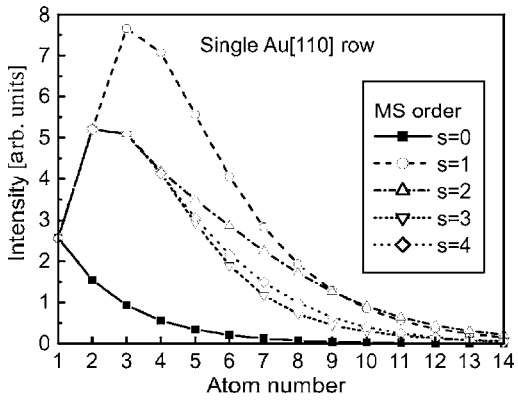

FIG. 3. Contribution of particular emitters of the [110] Au chain (Fig. 2) to the calculated intensity of elastically backscattered electrons [Eq. (6)] for the zeroth, first, second, third, and fourth maximum scattering orders. E_P=1.0 keV, λ=13.0 Å, T=300 K, bond distance 2.88 Å.

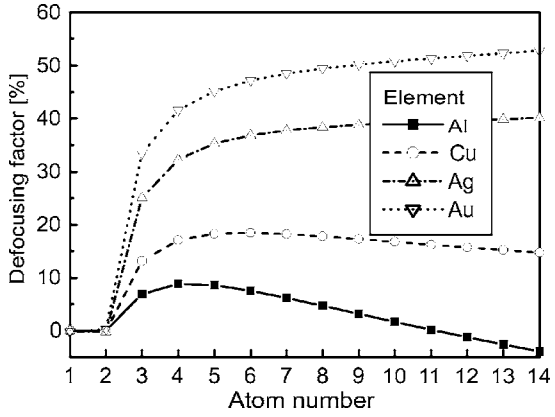

FIG. 4. Defocusing factor $100\% \times (I_{SS}-I_{MS})/I_{SS}$ (see text) versus particular emitters in the chain obtained for elements Al, Cu, Ag, and Au.

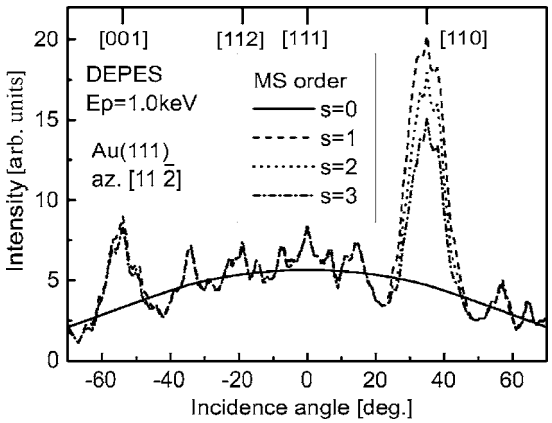

FIG. 6. Theoretical DEPES polar profiles at $E_P=1.0$ keV for Au(111) and the $[11\bar{2}]$ azimuth calculated with the use of the MS approach for maximum scattering orders from $s=0$ to 3.

tion ($\theta_k=0°$) parallel to the [110] close-packed row of atoms (Fig. 2). In Fig. 3 the calculated intensities of elastically backscattered electrons are presented as a function of the emitter number for given maximum scattering orders s along the [110] chain of Au atoms. When no scattering takes place ($s=0$), an exponential decrease of the calculated intensities with the emitter number (Fig. 2) is observed as a result of the damping of primary and emitted electrons. Single scattering of the primary electron wave ($s=1$) leads to the increase of signal contributions of the first few atoms in the chain. Then a decrease of the calculated signal is observed for further emitters along the chain. Multiple scattering events ($s>1$) give the same result for the second atom in the chain as in the case of single scattering ($s=1$), due to the presence of only one scatterer above the second layer. The consideration of multiple scattering leads to the reduction of calculated intensities for further emitters in the chain. No significant differences in calculated intensities were found above the fourth scattering order. The calculations performed for Al, Cu, and Ag confirm the above considerations.

For fixed incidence direction ($\theta_k=0°$ in Fig. 2) no significant changes of calculated intensities from one [110] chain were found when the presence of the neighboring [110] atomic rows was taken into account in calculations. An analysis of the theoretical data obtained for the [110] atomic chain for the (111) face (fixed $\theta_k \approx 35°$) leads to similar conclusions. The above effect results from the anisotropic scattering amplitude, which is the highest along the forward direction. For higher scattering angles a rapid decrease of the scattering amplitude is noted, which leads to the minor contribution of the neighboring [110] chains to the calculated intensity from one [110] row.

In Fig. 4 the effect of MS defocusing associated with emitters along the [110] chain (Fig. 2) is presented. The defocusing factor is defined as $100\% \times (I_{SS}-I_{MS})/I_{SS}$, where I_{SS} and I_{MS} are the intensities calculated for parameter $s=1$ and $s=9$, respectively. A clear dependence of the defocusing factor on the considered Al, Cu, Ag, and Au elements is observed, which was previously reported in the case of x-ray photoelectron and Auger electron diffraction.[30] A strong depression of the calculated intensities was found for Ag and Au atoms due to the large elastic scattering cross section of these atoms. Therefore, the MS events are expected to play an important role in the measured DEPES profiles for these elements. A similar analysis performed for Al and Cu reveals

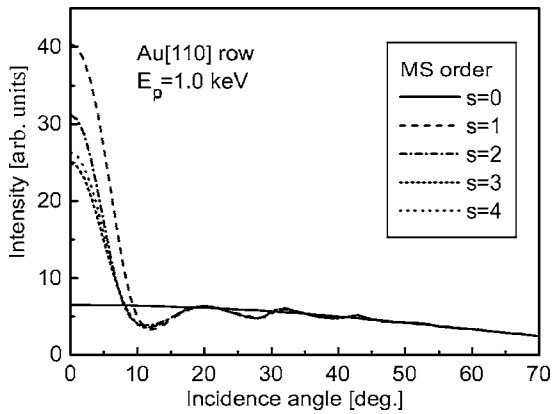

FIG. 5. Calculated intensity of elastically backscattered electrons [Eq. (7)] for the [110] chain of Au atoms (Fig. 2) and maximum scattering orders from $s=0$ to 4 as a function of the incident angle θ_k of the primary electron beam.

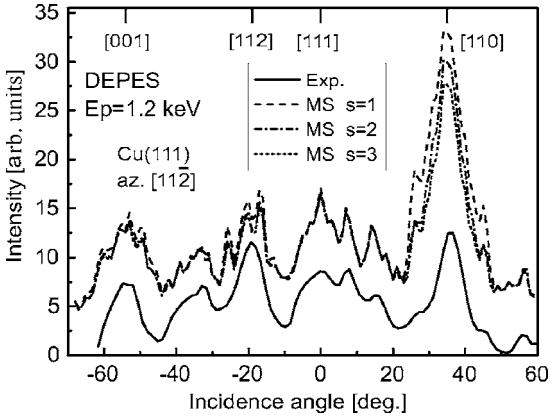

FIG. 7. Experimental DEPES profile for Cu(111) at $E_P=1.2$ keV in the $[11\bar{2}]$ azimuth and theoretical scans obtained with the use of the MS approach for scattering orders $s=1$, 2, and 3.

a significantly weaker defocusing effect. For Al even an increase of MS intensities for deeper layers is observed compared with single scattering calculations. In experiment we do not expect any influence of deeper layers on the measured signal due to the strong attenuation of primary and emitted electrons in a solid. The total intensity of elastically backscattered electrons as a function of the incidence angle of the primaries for the single Au[110] chain is presented in Fig. 5. When no scattering is taken into account ($s=0$) a continuous decrease of calculated intensities is observed due to the attenuation of primary and emitted electrons. For $s=1$ enhancement of intensities is noted for the incidence angle parallel to the [110] direction, which is associated with the forward scattering of the primaries. Higher scattering orders ($s=2$, 3, and 4) lead to the depression of the [110] intensity maximum, which is associated with the defocusing of primaries. Above $s>3$, no significant changes of calculated intensities were observed. This analysis shows the importance of multiple scattering events for calculated intensities of elastically backscattered electrons. The calculations performed for the family of [110] atomic rows prove that the calculated intensities are mainly affected by the forward scattering of the primary wave. The presence of other scattering atoms belonging to the neighboring [110] chains does not affect significantly the calculated intensities for one chain, which results from the small scattering amplitude associated with large scattering angles.

The MS approach was used to obtain DEPES profiles for Au(111) and the $[11\bar{2}]$ azimuth at $E_P=1.0$ keV (Fig. 6). Different scattering orders from $s=0$ to 3 were taken into account in calculations. When no scattering of the primary wave is considered ($s=0$) the isotropic profile is observed. The decrease of the calculated intensities with the incidence angle is associated with the attenuation of the primary and emitted electrons along their way in the sample. For $s=1$ the [001] and [110] intensity maxima are very well visible in the calculated DEPES profile. Depression of the [110] maximum is observed for the second and third scattering order, as was observed previously for the single Au[110] chain of atoms (Fig. 5). The MS events do not influence significantly the calculated intensities for the [001], [112], and [111] rows of atoms.

Experimental DEPES profile for Cu(111) at $E_P=1.2$ keV and theoretical scans obtained for scattering orders $s=1$, 2, and 3 are presented in Fig. 7. Better correspondence between experimental and theoretical data was found when higher scattering orders were considered in the MS calculations. The reduction of calculated intensities for the close-packed [110] direction with the scattering order is observed, as was previously noted for Au(111). The data presented in Fig. 6 and 7 show also that the MS events do not influence significantly the intensities for other incidence angles. The presented results show the importance of multiple scattering events of primary electrons in the crystalline sample for the creation of the elastically backscattered electron intensities observed in DEPES profiles.

V. CONCLUSIONS

The above presented data show the significance of multiple scattering effects in calculated DEPES profiles. In calculations the scattering of the primary plane wave is considered, which is associated with the diffraction effects of the primary electron beam in the crystalline sample. The multiple scattering and the attenuation of primary and emitted electrons in the sample cause the information depth about the crystalline structure of the sample to reach a few atomic layers. The MS events of primary electrons cause the depression of the intensity maxima in the DEPES profiles corresponding to the [110] close-packed row of atoms. This depression leads to a better correspondence between experimental and theoretical data, which can be used in the quantitative analysis of the results. The data obtained for the Au(111) crystal confirm the results for the single Au[110] chain of atoms, where no significant changes of the calculated intensities in DEPES were found above the third scattering order. The results obtained for the Au[110] chain of atoms suggest that the calculated intensities are mainly affected by the forward scattering along the close-packed rows. The scattering atoms of the neighboring [110] rows do not affect significantly the calculated intensities. A better correspondence between theoretical and experimental data was found for higher scattering orders. To our best knowledge, the MS approach for the primary plane wave used for DEPES has been presented in this paper for the first time.

ACKNOWLEDGMENTS

We are indebted to Stefan Mróz for numerous discussions. We acknowledge the support of the University of Wrocław under Grant No. 2016/W/IFD/2006 and of the European Social Fund within the Project of Lower Silesia Research Grants for increasing innovations for Ph.D. students, No. Z/2.02/II/2.6/04/04/U/03/05/. Calculations have been carried out in Wrocław Center for Networking and Supercomputing.

*Electronic address: nowicki@ifd.uni.wroc.pl

[1] P. Morin, Surf. Sci. **164**, 127 (1985).
[2] D. G. Coates, Philos. Mag. **16**, 1179 (1967).
[3] Y. Sakai and A. Mogami, J. Vac. Sci. Technol. A **5**, 1222 (1987).
[4] H. E. Bishop, Surf. Interface Anal. **16**, 118 (1990).
[5] T. W. Rusch, J. P. Bertino, and W. P. Ellis, Appl. Phys. Lett. **23**, 359 (1973).
[6] M. V. Gomoyunova, S. L. Dudarev, and I. I. Pronin, Surf. Sci. **235**, 156 (1990).
[7] H. C. Poon and S. Y. Tong, Phys. Rev. B **30**, 6211 (1984).
[8] A. Stuck, M. Nowicki, S. Mróz, D. Naumović, and J. Osterwalder, Surf. Sci. **306**, 21 (1994).
[9] M. Nowicki and J. Osterwalder, Surf. Sci. **408**, 165 (1998).
[10] C. H. Li and S. Y. Tong, Phys. Rev. Lett. **43**, 526 (1979).
[11] S. Y. Tong, H. C. Poon, and D. R. Snider, Phys. Rev. B **32**, 2096 (1985).

[12] M. L. Xu, J. J. Barton, and M. A. Van Hove, Phys. Rev. B **39**, 8275 (1989).
[13] W. F Egelhoff, Phys. Rev. Lett. **59**, 559 (1987).
[14] S. Mróz and M. Nowicki, Surf. Sci. **297**, 66 (1993).
[15] M. Nowicki, Vacuum **54**, 73 (1999).
[16] M. Nowicki, Phys. Rev. B **69**, 245421 (2004).
[17] J. J. Barton and D. A. Shirley, Phys. Rev. B **32**, 1906 (1985).
[18] J. J. Barton, M. L. Xu, and M. A. Van Hove, Phys. Rev. B **37**, 10475 (1988).
[19] V. Fritzsche, J. Electron Spectrosc. Relat. Phenom. **58**, 299 (1992).
[20] V. Fritzsche, O. Knauff, and H. P. Bonzel, Phys. Rev. B **49**, 10643 (1994).
[21] F. J. Garcia de Abajo, M. A. Van Hove, and C. S. Fadley, Phys. Rev. B **63**, 075404 (2001).
[22] P. A. Lee and J. B. Pendry, Phys. Rev. B **11**, 2795 (1975).
[23] J. B. Pendry, *Low Energy Electron Diffraction* (Academic Press, London, 1974).
[24] J. J. Rehr and R. C. Albers, Phys. Rev. B **41**, 8139 (1990).
[25] T. Konga, K. Kanayama, S. Watanabe, and A. J. Thakkar, Int. J. Quantum Chem. **71**, 491 (1999).
[26] T. Konga, K. Kanayama, T. Watanabe, T. Imai, and A. J. Thakkar, Theor. Chem. Acc. **104**, 411 (2000).
[27] D. J. Friedman and C. S. Fadley, J. Electron Spectrosc. Relat. Phenom. **51**, 689 (1990).
[28] Y. Gao and J. Cao, Phys. Rev. B **43**, 9692 (1991).
[29] S. Tanuma, C. J. Powell, and D. R. Penn, Surf. Interface Anal. **17**, 911 (1991).
[30] H. A. Aebischer, T. Greber, J. Osterwalder, A. P. Kaduwela, D. J. Friedman, G. S. Herman, and C. S. Fadley, Surf. Sci. **239**, 261 (1990).